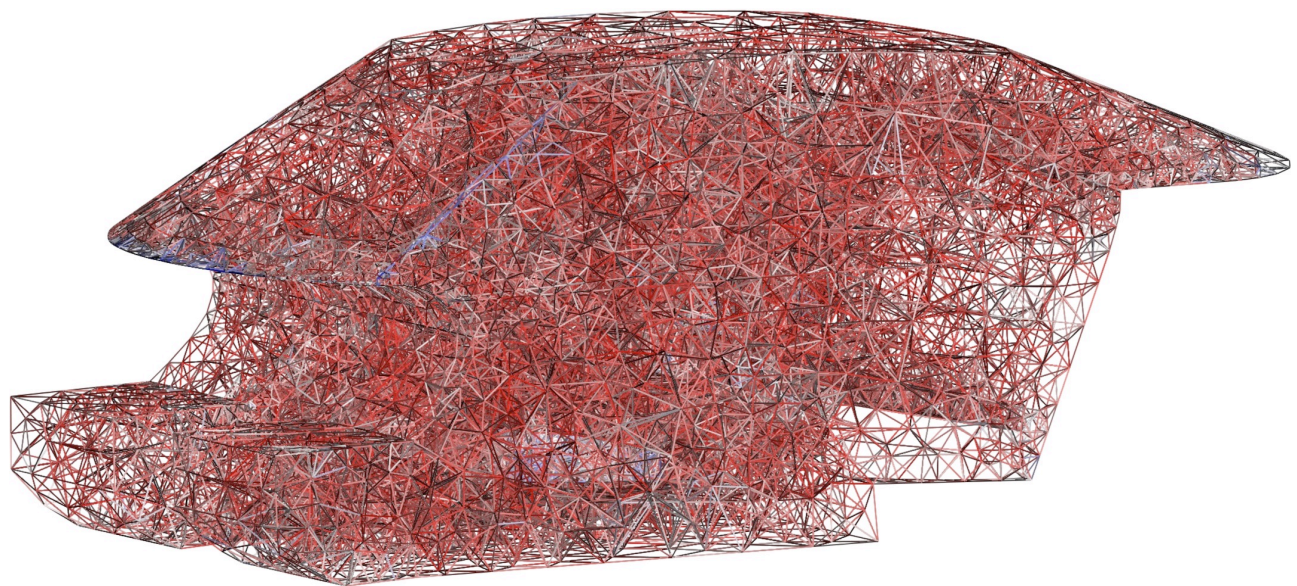


# CHALMERS



## A FEM model for simulating reflection of sound by a car compartment's windscreen and lateral front windows

Master's Thesis in the Master's programme in Sound and Vibration

**EDMUNDO GUEVARA FLORES**

Department of Civil and Environmental Engineering  
*Division of Applied Acoustics*  
*Chalmers Room Acoustics Group*  
CHALMERS UNIVERSITY OF TECHNOLOGY  
Göteborg, Sweden 2013  
Master's Thesis 2013:63



# A FEM model for simulating reflection of sound by a car compartment's windscreen and lateral front windows

Master's Thesis in the Master's Programme in Sound and Vibration

EDMUNDO GUEVARA FLORES

Department of Civil and Environmental Engineering

*Division of Applied Acoustics*

*Chalmers Room Acoustics Group*

CHALMERS UNIVERSITY OF TECHNOLOGY

Göteborg, Sweden 2013

A FEM model for simulating reflection of sound by a car compartment's  
windscreen and lateral front windows

Master's Thesis in the Master's programme in Sound and Vibration

© EDMUNDO GUEVARA FLORES, 2013

Master's Thesis 2013:63  
Department of Civil and Environmental Engineering  
*Division of Applied Acoustics*  
*Chalmers Room Acoustics Group*  
Chalmers University of Technology  
SE-412 96 Göteborg  
Sweden  
Telephone: + 46 (0)31-772 2200

Cover:  
Mesh of the passenger compartment model D,  
3 elements per wavelength @ 500 Hz

Reproservice / Department of Civil and Environmental Engineering  
Göteborg, Sweden 2013

# **A FEM model for simulating reflection of sound by a car compartment's windscreen and lateral front windows**

Master's Thesis in the Master's Programme Sound and Vibration

EDMUNDO GUEVARA FLORES

Department of Civil and Environmental Engineering

*Division of Applied Acoustics*

*Chalmers Room Acoustics Group*

Chalmers University of Technology

## **ABSTRACT**

A nearly undisturbed communication between passengers is a desired target for good vehicle acoustics. For speech intelligibility inside car interiors, the early reflections caused by the lateral front windows and the windscreen seem to play an important role. Therefore, a suitable simulation model would enhance possibilities of developing acoustically optimized interiors. However most of the speech information is contained in the frequency range between 400 Hz and 6 kHz, making challenging the use of numerical methods like finite element or boundary element analyses, where the accuracy depends highly in the amount of elements per wavelength. On the other hand the size and speed of today computers might provide an opportunity to overcome some limitations.

The goal of this project was to design a Finite Element Model of a simplified car interior in order to identify how early reflections are influenced by changes in the side windows and windshield geometries. Four models based on the Saab 9-3 passenger compartment were created. The windshield and lateral front windows were modeled as sound-hard acoustic boundaries, whereas all the other surfaces were modeled as absorptive. The frequency range under study goes from 100 Hz up to 3.5 kHz, with a frequency step of 50 Hz that allowed generating a causal impulse response of 0.02 seconds.

The results show that it is possible to get information on how the early reflections are affected by changes in the geometry. However, the results were not only affected by changes in geometry but also by the boundary conditions specified in the simulations.

Key words: FEM (Finite Element Method), Car Compartment, Impulse Response, Car windows, Room Acoustics



# Contents

<b>ACKNOWLEDGMENTS</b>	<b>3</b>
<b>1. INTRODUCTION</b>	<b>4</b>
Objective	5
<b>2. BACKGROUND</b>	<b>6</b>
Governing Equations	7
Finite Element Formulation	10
COMSOL Multiphysics® Time-harmonic Analysis	12 12
Butterworth Filters	14
<b>3. SETUP AND PARAMETERS</b>	<b>17</b>
Enclosed Air Space, 2D Model	17
Passenger Car Compartment 3D Models	18
Simulation Settings	21
Mesh	21
Boundary Conditions	22
Source	22
Solver	22
Post-processing	23
Low-pass Butterworth filter design	23
<b>4. RESULTS</b>	<b>26</b>
Enclosed Air Space 2D Model	26
Passenger Car Compartment 3D Models	27
<b>5. DISCUSSION</b>	<b>28</b>
<b>6. CONCLUSIONS</b>	<b>30</b>
<b>7. FUTURE WORK</b>	<b>31</b>
<b>8. REFERENCES</b>	<b>33</b>
<b>APPENDIX A CAR COMPARTMENT GEOMETRIES</b>	<b>36</b>



# Acknowledgments

The technical support of SAAB/Opel (GM) is kindly acknowledged. The author also thanks Prof. Mendel Kleiner and Börje Wijk at the department of Applied Acoustics, Chalmers, for their continuous support and help.

Göteborg February 2013

Edmundo Guevara Flores

# 1. Introduction

Comfort, safety and security are important while driving a car, as is undisturbed communication between passengers and driver. However the noise and the sound absorptive environment inside the car compartment makes such communication difficult to achieve. Expensive cars have sound absorptive treatment to help reduce the noise levels but such treatment also affects the speech sounds by reducing their strength. For good speech intelligibility inside car interiors, the early reflections caused by the lateral front windows and the windscreen play an important role.

Speech covers the frequency range from about 0.125 to 8 kHz with most of the information content centred around 0.5 to 2 kHz. Speech intelligibility can be shown to increase in auditoria with increasing reverberation time for very short reverberation times in the range of up to about 0.6 s. Typical compartment reverberation time may however have values as low as 0.04 s. For such low values the early reflections by the windows support speech intelligibility because they contribute to an improved signal to noise ratio. Early reflections by the windows also help overcome the influence of speaker sound radiation directivity. To reflect sound efficiently a window must be large enough to be covered by several Fresnel zones.

Because of the small size of these reflecting surfaces early reflections cannot be adequately modelled using ray tracing, instead a suitable finite element based simulation model would improve the possibilities of studying the influence of the hard surfaces on the room impulse response of the car interior.

# Objective

The main goal of this project was to design a Finite Element Model (FEM) of a simplified car interior, consisting of a seat, a windscreen and the lateral (side) front windows. The influence of different parameters, like window size or windscreen slope, was investigated. Figure 1 shows the main tasks performed in this project in order to achieve the goal.

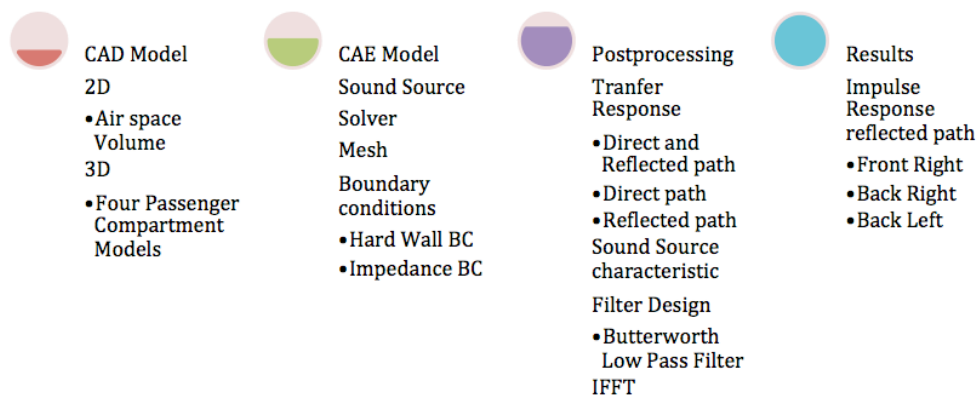


*Figure 1: Overview of the project.*

## 2. Background

The finite element method (FEM) is a numerical analysis approach employed to give approximate solutions to problems governed by partial differential equations.

Even though FEM has been applied many times to find solutions to acoustical problems, it has seldom been used to estimate room impulse response. Most of the work done using FEM has been focused on analysis of the structure-acoustic relation and to estimate modes and frequencies of the passenger compartment

The FEM approximation is obtained by means of searching a solution within the mathematical space defined by a set of trial functions, each of which differs from zero only in a small part of the domain – an element. As a consequence of such a selection of trial functions, it is easy to follow complex geometry and it is possible to vary material properties from element to element [3].

The finite element method is applied using the following steps:

1. Discretize the continuum
2. Select interpolation functions
3. Find the element properties
4. Assemble the element properties to obtain the system equations
5. Impose the boundary conditions
6. Solve the system equations
7. Make additional computations if desired

## Governing Equations

Let us consider a three-dimensional lossless acoustic cavity  $\Omega$  ( $m^3$ ), surrounded by the boundary surface  $\Gamma = \partial\Omega$  ( $m^2$ ) as depicted in Figure 1. At point  $Q$  a monopole source excites the medium. Then, the acoustic pressure of sound waves at receiver point  $P$  inside the volume  $\Omega$  is governed by:

$$\nabla \cdot \left( \frac{\nabla p}{\rho} \right) + \frac{1}{\rho c_s^2} \frac{\partial^2 p}{\partial t^2} = -Q \quad \text{in } \Omega, \quad (2.1)$$

where  $c_s$  ( $m/s$ ) indicates to the speed of sound in the medium,  $\rho_0$  ( $kg/m^3$ ) denotes the density of the medium,  $Q$  ( $1/s^2$ ) refers to the monopole source.

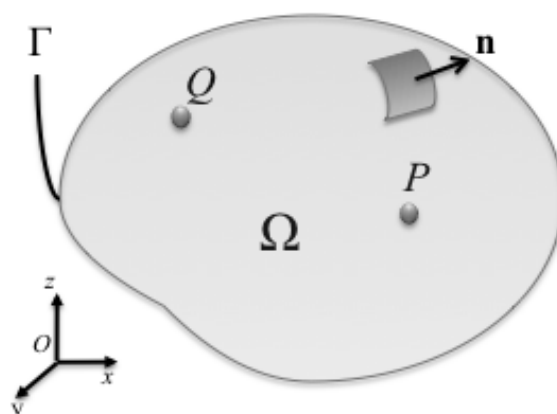


Figure 2: Lossless Acoustic Cavity Volume  $\Omega$  ( $m^3$ ), surrounded by surface  $\Gamma$  ( $m^2$ ).

Using the time-harmonic assumption, pressure  $p$  varies with time as:

$$p(\mathbf{r}, t) = \underline{\hat{p}}(\mathbf{r}) e^{j\omega t} \quad (2.2)$$

where  $\omega = 2\pi f$  ( $rad/s$ ) is the angular frequency,  $f$  ( $Hz$ ) the frequency, while  $S$  is the source amplitude,  $\delta^{(3)}(R)$  is the 3D Dirac delta function and  $R_0$  the position of the source. Finally, the wave equation (2.1) becomes, with the introduction of time-harmonic assumption, the inhomogeneous Helmholtz equation:

$$\Delta \underline{\hat{p}} + k^2 \underline{\hat{p}} = -\rho \underline{Q} \quad \text{in } \Omega, \quad (2.3)$$

where  $k=\omega/c_s$  is the wave number and  $\Delta$  is the Laplace operator. Since Helmholtz equation (2.3) is a second-order differential equation, one boundary condition needs to be specified at each point of the boundary in order to obtain a well-posed problem [4]. The boundary  $\Gamma=\partial\Omega$  ( $m^2$ ) is made up of three different non-intersecting surfaces  $\Gamma_{HB}$ ,  $\Gamma_{SB}$  and  $\Gamma_Z$ , so that

$$\begin{aligned} \Gamma &= \Gamma_{SB} \cup \Gamma_{HB} \cup \Gamma_Z \\ \Gamma_{SB} \cap \Gamma_{HB} &= 0 & \Gamma_{SB} \cap \Gamma_Z &= 0 & \Gamma_{HB} \cap \Gamma_Z &= 0 \end{aligned}$$

For every surface the boundary condition is defined as:

$$\begin{aligned} \text{Dirichlet BC:} & \quad \underline{\hat{p}}(\mathbf{r}) = \bar{p}(\mathbf{r}) \\ \text{Neumann BC:} & \quad \frac{\partial \underline{\hat{p}}}{\partial n} = -j\rho\omega \bar{v}_n \\ \text{Robin BC:} & \quad \frac{\partial \underline{\hat{p}}}{\partial n} = -\frac{j\bar{p}\rho\omega}{\bar{Z}} \end{aligned} \quad (2.4)$$

where  $n$  is the normal surface direction;  $\bar{p}$ ,  $\bar{v}_n$ ,  $\bar{Z}$  are prescribed values for acoustic pressure, normal velocity, and normal impedance. At an acoustically soft surface the acoustic pressure vanishes,  $\bar{p}=0$ , giving a pressure-release condition. For a sound-hard surface  $\bar{v}_n=0$ , the normal component of the particle velocity ceases because there is no acoustic drift velocity. The Robin boundary condition implies that the velocity at a point is only influenced by the pressure at that point and in some cases this is only a crude approximation to the truth [1].

The differential equations (2.3) and (2.4) can be represented, by applying the weighted residual method, as integral equations of the form:

$$\begin{aligned}
& \int_{\Omega} (\Delta \hat{p} + k^2 \hat{p} + \rho \underline{Q}) W d\Omega \\
& + \int_{\Gamma_{in}} \left( \frac{\partial \hat{p}}{\partial n} + j\rho\omega \bar{v}_n \right) W d\Gamma_{in} \\
& + \int_{\Gamma_z} \left( \frac{\partial \hat{p}}{\partial n} + \frac{j\hat{p}\rho\omega}{Z} \right) W d\Gamma_z = 0
\end{aligned} \tag{2.5}$$

where  $W$  represents weighting functions. Notice that Neumann and Robin boundary conditions are now included in the functional, therefore only Dirichlet boundary condition has to be satisfied.

By using Green's formulae, equation (2.5) can be written as a weak form:

$$\begin{aligned}
& \int_{\Omega} \left( -(\nabla W)^T (\nabla \hat{p}) + k^2 W \hat{p} + \rho W \underline{Q} \right) d\Omega \\
& + \int_{\Gamma_{in}} j\rho\omega \bar{v}_n W d\Gamma_{in} + \int_{\Gamma_z} \frac{j\hat{p}\rho\omega}{Z} W d\Gamma_z = 0
\end{aligned} \tag{2.6}$$

The weak form is more 'permissive' and realistic, from a physical point of view, than the original problem defined by equations (2.3) and (2.4). The two previous integral statements will form the basis of finite element approximations [20].

## Finite Element Formulation

The three-dimensional acoustic cavity,  $\Omega$  ( $m^3$ ), enclosed by surface  $\Gamma = \partial\Omega$  ( $m^2$ ) is divided into a discrete quantity of non-overlapping finite elements, FE mesh. Each element, denoted as  $\Omega_e$ , is bounded by four surfaces defined as:

- $\Gamma_{e_{SB}}, \Gamma_{e_{HB}}, \Gamma_{e_Z}$ : The boundary of the element  $\Omega_e$  is the boundary of the domain  $\Omega$ .
- $\Gamma_{e_K}$ : Boundary between two adjacent elements

The weak form for one element can be written as:

$$\int_{\Omega_e} \left( -(\nabla W)^T \nabla \hat{p}_e + k^2 W \hat{p}_e + \rho W Q \right) d\Omega_e + \int_{\Gamma_{SB}} j\rho\omega \bar{v}_s W d\Gamma_{SB} + \int_{\Gamma_Z} \frac{j\hat{p}_e \rho\omega}{Z} W d\Gamma_Z + \int_{\Gamma_K} j\rho\omega v_i W d\Gamma_K = 0 \quad (2.7)$$

where  $v_i$  is the unknown interface velocity, which must be continuous at  $\Gamma_{e_K}$ .

The pressure within each element  $\Omega_e$  can be approximated by:

$$\hat{p}_e = \sum_{a=1}^n N_a \hat{p}_{ea} = \mathbf{N} \hat{\mathbf{p}}_{ea} \quad (2.8)$$

where  $p_a$  are nodal pressure values associated with known shape functions  $N_a$ . However, the previous approximation, equation (2.8), fails to comply with Helmholtz equation (2.3) and boundary conditions (2.4). Hence it is important to introduce another approximation. Using the Galerkin approach the weighting function  $W$  will be:

$$W = \sum_{b=1}^n N_b \delta \hat{p}_{eb} = \mathbf{N}_b \delta \hat{\mathbf{p}}_{eb} \quad (2.9)$$

in which  $\delta \hat{\underline{p}}_{en}$  are arbitrary nodal parameters therefore it is sufficient to determine the parameters  $\hat{\underline{p}}_{en}$  [20]. In the Galerkin method the weighting functions are the original shape functions,  $\mathbf{w}_b = \mathbf{N}_b$ .

The substitution of both approximations in the weak form (2.7) yields a linear system of equations of the form:

$$\left(-\omega^2 \mathbf{M}_e + j\omega \mathbf{C}_e + \mathbf{K}_e\right) \hat{\underline{p}}_e = j\omega \left(\underline{\mathbf{Q}}_e - \mathbf{v}_n - \mathbf{v}_i\right) \quad (2.10)$$

$$\begin{aligned} \mathbf{M}_e &= \int_{\Omega_e} \frac{\mathbf{N}_b^T \mathbf{N}_b}{c_s^2} d\Omega_e && \text{Acoustic Mass Matrix} \\ \mathbf{C}_e &= \int_{\Gamma_{e,z}} \left(\frac{\rho}{Z}\right) \mathbf{N}_b^T \mathbf{N}_b d\Gamma_{e,z} && \text{Acoustic Damping Matrix} \\ \mathbf{K}_e &= \int_{\Omega_e} \left(\nabla \mathbf{N}_b\right)^T \left(\nabla \mathbf{N}_b\right) d\Omega_e && \text{Acoustic Stiffness Matrix} \\ \underline{\mathbf{Q}}_e &= \int_{\Omega_e} \rho \mathbf{N}_b^T \underline{Q} d\Omega_e && \text{Source Term Matrix} \\ \mathbf{v}_{en} &= \int_{\Gamma_{e,ns}} \rho \mathbf{N}_b^T \bar{v}_n d\Gamma_{e,ns} && \text{Normal Velocity Matrix} \\ \mathbf{v}_{ei} &= \int_{\Gamma_{e,i}} \rho \mathbf{N}_b^T \bar{v}_i d\Gamma_{e,i} && \text{Adjacent Elements BC Matrix} \end{aligned}$$

The assembly of all the elements will result in the global Finite Element Model.

## COMSOL Multiphysics®

The practical simulation work in this project was carried out using the Acoustics Module in the COMSOL Multiphysics® software v. 3.6. This module contains a built-in application mode named Pressure Acoustics; that allows modelling in a fluid using four distinct PDE formulations:

- Transient analysis. Acoustic modelling using the wave equation.
- Time-harmonic analysis. Acoustic modelling using the inhomogeneous Helmholtz equation.
- Eigenfrequency analysis. Acoustic modelling using the homogeneous Helmholtz equation.
- Modal analysis. Eigenmode analysis on boundaries of acoustic propagating through the boundary.

In all analyses the dependent variable is the acoustic pressure,  $p$ .

It has been demonstrated that the sound field inside an acoustic cavity can be described by means of the inhomogeneous Helmholtz equation; therefore the analysis that best suited the work carried out in this project was Time-harmonic.

### Time-harmonic Analysis

As previously stated, with Time-harmonic analysis the software solves the inhomogeneous Helmholtz equation:

$$\nabla \cdot \left( -\frac{1}{\rho} (\nabla p - \mathbf{q}) \right) - \frac{\omega^2}{\rho c_s^2} p = Q \quad (2.11)$$

where  $p$  is pressure, dependent on position  $r$  and frequency  $f$ ;  $\omega=2\pi f$  is angular frequency defined in terms of frequency  $f$ ;  $c_s$  is speed of sound in the medium;  $\rho_0$  is the fluid density;  $\mathbf{q}$  is dipole source; and  $Q$  is monopole source.

The analysis is done in the frequency domain; therefore the Frequency Response Function (FRF) can be determined by sweeping over a suitable frequency range. To do so it is necessary to specify the lower and higher frequency limits, together with the frequency step.

It is possible to assign values or expressions to every independent variable. Also, the system allows the use of matrices when the variable of interest changes with respect to another variable specified in the system. For instance, when the impedance of a surface varies with respect to frequency.

Various ways are available to account for the damping in the medium. For Complex Material, a complex impedance and complex wave number are required. In the General Damping option it is necessary to specify an attenuation coefficient. The flow resistivity is needed when the Delaney-Bazley choice is selected. Bulk Viscosity is the final alternative; in this case the bulk viscosity is expected. In the last three types of damping, the software determines a complex wave number and complex impedance, values provided by the user with the Complex Material selection. With these data a complex speed of sound and complex fluid density are calculated and used as inputs in the inhomogeneous Helmholtz equation.

An alternative to model absorption properties is the Perfectly Matched Layer (PML) formulation. The PML is not considered a boundary condition but an extra domain that absorbs the incident sound. The available PML types are Cartesian, cylindrical, spherical and an option where the user defines the PML coordinates by means of expressions or values in  $x$ ,  $y$  and  $z$ .

The software uses Lagrange-quadratic elements as default option, however Lagrange-linear, Lagrange-cubic and Lagrange-quartic can be selected instead.

Inside the Pressure Acoustics mode different boundary conditions are available. The Sound-Hard boundary condition must be used to model rigid acoustic surfaces. If the acoustic pressure vanishes at the boundary then the Sound-Soft boundary condition needs to be selected. The Pressure Source boundary condition allows specifying the acoustic pressure at a boundary.

With the Normal Acceleration boundary condition an inward normal acceleration that represents an external source is required. As the name indicates, the input of the Impedance boundary condition is the acoustic impedance of an external domain. For the Radiation boundary condition, an outgoing wave that leaves the domain can be modelled as Plane, Cylindrical or Spherical. The Matched boundary condition gives the opportunity to set up waves in ducts and waveguides.

Depending on its characteristic property, the strength of point sources can be specified in three ways. The Flow option allows setting the amplitude and complex phase of the source. Using the Intensity condition, a desired intensity at a precise distance can be stated. The total power a source would radiate is required when selecting the Power choice.

Different types of linear system solvers are included in COMSOL Multiphysics®. They are broadly categorized as direct or iterative solvers. The former includes UMFPACK, SPOLES, PARDISO and TAUCS; whereas GMRES, FGMRES, Conjugate Gradients, BiCGStab and Geometric Multigrid are found in the latter.

More detailed information can be found in references [35] and [36].

## Butterworth Filters

If the FEM solver is used to calculate the transfer function of the compartment the choice of upper and lower cutoff frequencies is very important in order to generate a causal impulse response. A causal impulse response cannot be obtained using a rapid “brick-wall” cutoff at either band edge. Using FEM it is easy to calculate to low frequencies. However high frequency calculations will be tedious since the use of the inverse Fourier transform to generate the impulse response from the transfer function requires the same frequency resolution at both high and low frequencies. Typically the transfer function is calculated with a frequency resolution of 1 Hz. To have a causal response the transfer function must be weighted using a suitable bandpass or high pass filter function that has little ringing. The FEM calculated transfer function can be considered a subset of transfer function extending to infinite frequency. Of

course the FEM calculated transfer function needs to be calculated up to several octaves over the cutoff frequency of any low pass filter used. Suitable filters are those having Bessel and Butterworth characteristic filters. In this work low pass Butterworth filter functions were used

Butterworth filters have a magnitude function

$$H(\omega) = \frac{1}{\sqrt{1 + \omega^{2n}}} \quad (2.12)$$

where  $\omega$  is the angular frequency and  $n$  the order of the filter.

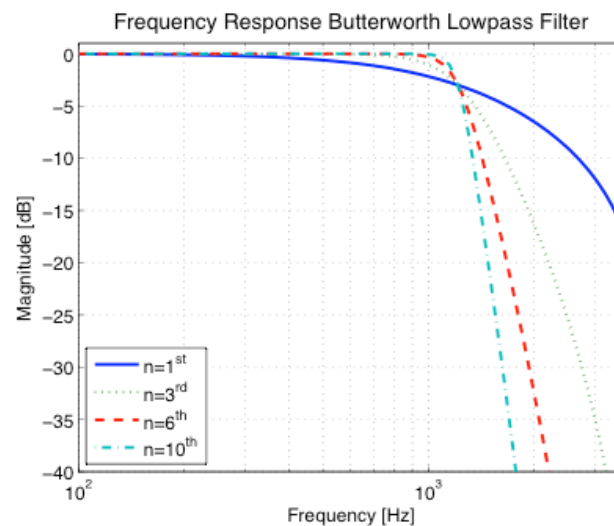


Figure 3: Gain of 1st, 3rd, 6th and 10th orders low-pass Butterworth filters.

Figure 3 shows the gain in dB of four low-pass Butterworth filters. The filters do not exhibit ripples in the passband, consequently its response is flat and for that reason they are commonly called *maximally flat filters*. The roll-off from the passband to the stop band is determined by the order of the filter. As the order increases towards infinity the slope becomes sharper and approaches to the ideal filter response that exhibits a rectangular shape.

The most important step when designing a low-pass Butterworth filter is to determine the desired order  $n$ . The order of a IIR implementation of such a filter (using MatLab's signal processing toolbox) can be determined as follows:

$$n \geq \frac{\log_{10}(M)}{\log_{10}(\Omega)} = \frac{\ln(M)}{\ln(\Omega)} \quad (2.13)$$

$$\Omega \geq \frac{f_{stop}}{f_{pass}} \quad M = \sqrt{\frac{10^{0.1A_{stop}} - 1}{10^{0.1A_{pass}} - 1}} \quad (2.14)$$

where

$f_{stop}$  is the stopband frequency.

$f_{pass}$  is the passband frequency.

$A_{stop}$  is the maximum attenuation in decibels at the stopband.

$A_{pass}$  is the maximum passband reduction in decibels.

All these parameters are shown in figure 4.

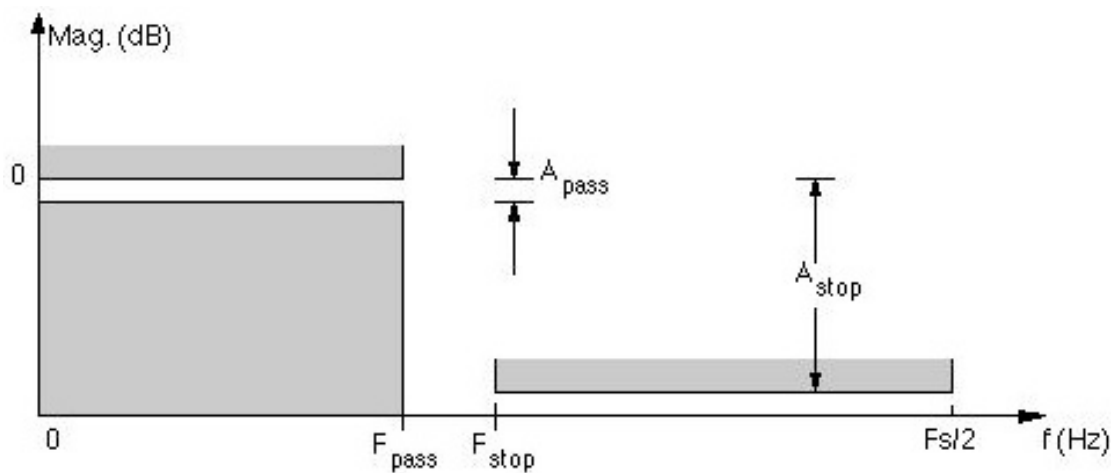


Figure 4: Filter specifications to design a Butterworth low-pass filter<sup>1</sup>.

<sup>1</sup> Filter Design & Analysis Tools (fdatool). Signal Processing Toolbox. MATLAB R2009b.

### 3. Chapter Three

## Setup and Parameters

### Enclosed Air Space, 2D Model

In order to study the boundary conditions behaviour and possible influence on the simulations of the 3D model, a 2D model representing an enclosed air space was created first.

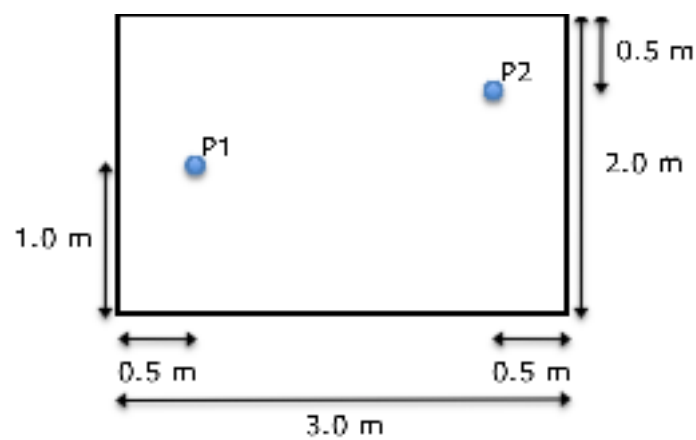


*Figure 5: Enclosed air space, 2D model. P1 is the sound source position, whereas P2 is the receiver position.*

The 2D sound field, shown in Figure 5, is a rectangle having the dimensions 3 x 2 m<sup>2</sup>. It consists of one point source, *P1*, located at (0.5, 1) m, and a receiver point, *P2*, positioned at (2.5, 1.5) m.

As a first approach all the boundaries were defined as absorptive using the impedance boundary condition. Thereafter the boundary at the horizontal bottom line was defined as Sound-hard boundary; whereas the vertical right line, horizontal top line and vertical left line remained as absorptive boundaries.

The frequency range of interest for calculation was from 100 Hz to 4 kHz. A frequency resolution of 5 Hz allowed obtaining an impulse response of .2 seconds much longer than necessary considering the car reverberation time.

## Passenger Car Compartment 3D Models

Saab provided four sets of NASTRAN files containing the meshed parts of the Saab 9-3 vehicle. Such data included extremely detailed geometries like the doors with all its components, the enclosed air volume, the pedals, and the car structure depicted in Figure 6, among others.

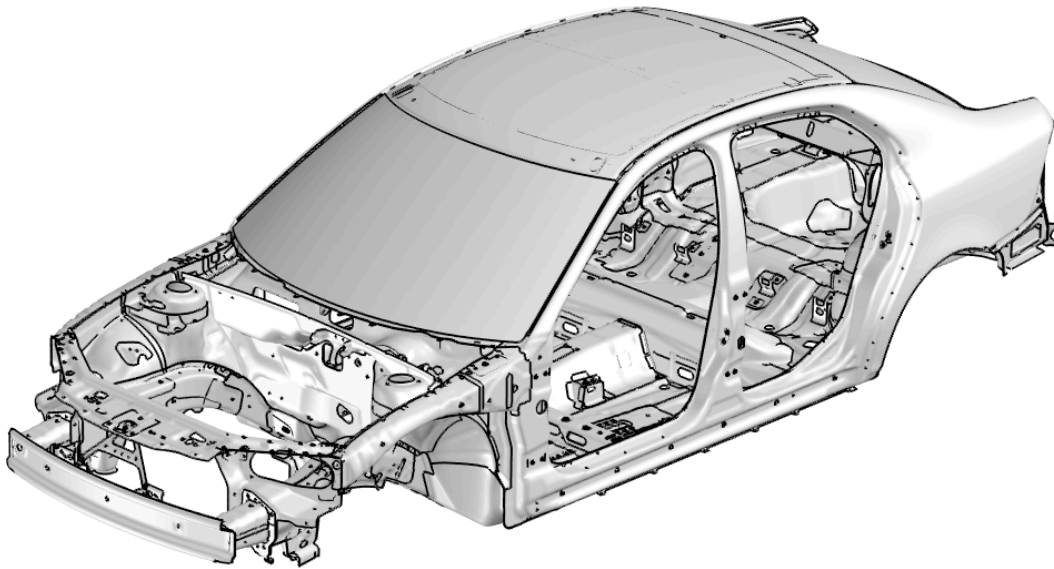


*Figure 6: NASTRAN mesh of the Saab 9-3 structure.*

Since the main objective of this thesis project was to investigate the early reflections produced by windshield and front side windows inside the automobile, it was indispensable to convert the meshed components into CAD objects in order to perform changes to the windshield and side windows geometries. This task is usually possible to do using COMSOL Multiphysics, since the software allows the import of NASTRAN meshes and, with a built-in command, converts meshed elements into objects. But in most of the cases it was not possible to import all the meshed elements to COMSOL Multiphysics because the software interpreted as error when two elements of one type coincided with one element of another type, for instance when one quadrilateral element coincided with two triangular elements. However all the meshed geometries were not essential to generate the 3D car cavity

models; only those having direct influence in the passenger compartment sound field were required.

The NASTRAN meshed elements of the enclosed air volume, seats, dashboard, central panel, and roof, windshield, side and rear windows were then imported to COMSOL Multiphysics. Figure 7 shows the geometries generated by COMSOL Multiphysics after being imported and transformed into objects. It is important to point out that detailed and small objects were avoided. Once the new 3D car compartment model was generated it was meshed again. In order to obtain a reasonable accuracy the new mesh had at least six elements per wavelength; this means that the maximum element size was  $\lambda/6$ . Therefore as the frequency increased, the number of elements went up too, resulting in a finer mesh that demanded more computational work, RAM memory, and represented farther calculation time.

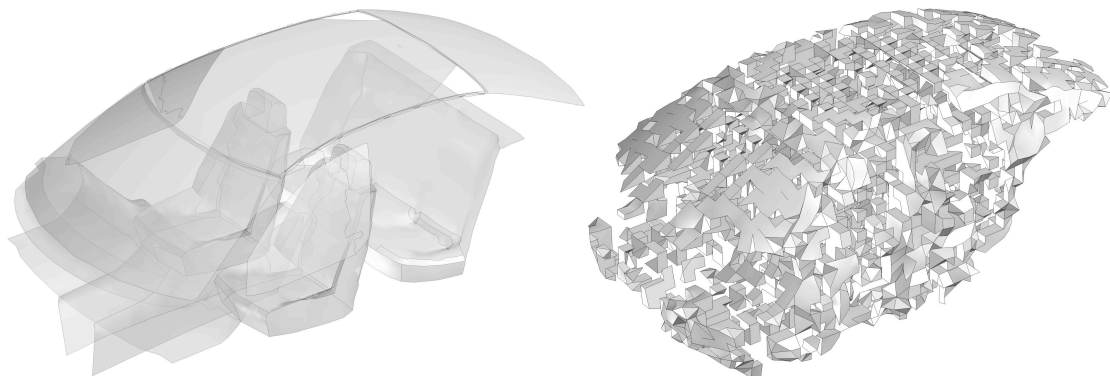


*Figure 7: Windshield, roof, seats, dashboard, central panel and windows in the passenger compartment (Left side). Enclosed air volume (Right side).*

Two windshields and two side windows were generated. One windshield is “straight” and the other “curved”. In the same way one pair of side windows is “straight” and the other pair is “curved”. With the combination of side windows and windshields four 3D passenger compartment models were obtained. The models were necessary to evaluate how the early reflections changed in accordance to changes in the geometry of side windows and windshield.

- Model A (Figure A1). Flat side windows and flat windshield.
- Model B (Figure A2). Flat side windows and curved windshield.
- Model C (Figure A3). Curved side windows and flat windshield.
- Model D (Figure A4). Curved side windows and curved windshield.

Each model is a simplified representation of a Saab 9-3 passenger compartment. Figure 5 illustrates the differences between the original mesh and one of the models. It is possible to observe that the original mesh is more complex and has more details than the simplified model generated for this project.

A point source was located at the front left (FL) inside the passenger compartment, whereas three receiver points were positioned at the front right (FR), back left (BL) and back rights (BR) places in the interior. The Cartesian coordinates for each position are shown in Table 1.

*Table 1 Cartesian coordinates of the source and receivers points located inside de passenger compartment.*

	x	y	Z
Source (FL)	3,21	-0.36	1.05
Receiver 1 (FR)	3,21	0.36	1.05
Receiver 2 (BL)	3,99	-0.36	1.05
Receiver 3 (BR)	3,99	0.36	1.05

As a first approach, the surfaces considered as windshield and side windows were supposed as totally reflective, therefore set as hard-sound boundaries; whereas an impedance boundary condition was selected for all the other surfaces, which were assumed as totally absorptive and defined by means of the complex impedance obtained from the porous absorber model implemented in Matlab. The task of this configuration was to obtain the acoustic pressure of sound waves reflected by the side windows and the windshield together with the direct sound waves arriving at each one of the receiver positions.

Thereafter, in order to obtain only the direct sound, the configuration was changed. Using the impedance boundary condition, all the surfaces were considered as absorptive.

With the results of the previous approaches it was possible to get the sound waves reflected from the windshield and side windows without the influence of the direct sound.

The FEM simulations were performed over the frequency range from 50 Hz to 3.5 kHz, with a frequency step of 50 Hz that allowed calculating an impulse response of .02 seconds.

## Simulation Settings

Parametric sweep was performed to get results over the frequency range of both models. For the 2D model the sweep was carried out over all the frequency range at once. For the 3D model the sweep was executed in steps, this helped to reduce the calculation time because the mesh depends highly on the upper frequency limit of each sweep. The first step covered the frequency range from 50 Hz to 2 kHz; the second step went from 2 kHz to 3 kHz; in the last step, from 3 kHz to 3.5 kHz, the upper frequency limit was reached.

All simulations of this study were ran on a computer with 8 Intel® Xenon® processors @ 2.00 GHz and a total available RAM memory of 46.6 gigabytes.

## Mesh

Maximum element size:  $\lambda/3$ . Commonly accepted  $\lambda/6$ , but the Geometric Multigrid solver allows using a lower number of elements per wavelength.

## Boundary Conditions

Sound-Hard Boundary (Wall).

Impedance Boundary Condition.

## Source

Point source for the acoustic pressure field. Defined by means of its flow strength. For both models the flow value is  $1e^{-5}$  ( $m^3/s$ ).

## Solver

The 3D model resulted to be large, from the point of view of FEM, therefore it required the use of three iterative solvers and one direct solver.

### **FGMRES**

This iterative solver was selected as the linear system solver

### **Geometric Multigrid**

Selected as preconditioner because the linear system solver is an iterative solver that requires the use of preconditioners.

### **GMRES**

The preconditioner needed both a presmoothing and a postsmoothing, therefore GMRES was selected without preconditioners.

### **Pardiso**

The preconditioner also needs a coarse solver, hence Pardiso was the option selected.

## Post-processing

The post-processing of data obtained with the FEM model was carried out with Matlab. The simulation results, real and imaginary parts of the acoustic pressures were exported to the previously mentioned software. To obtain the frequency response of the reflected path

Then, the sound source characteristic was taken into account to obtain a flat transfer response. Thereafter a Butterworth low-pass filter was designed and applied to the previous results. Finally, using the inverse Fourier transform, it was possible to find the causal impulse response.

### Low-pass Butterworth filter design

To eliminate the non-causality present in the IR, two Butterworth Low-pass filters were implemented. One was applied to the results obtained from the 2D model simulation, while the other was employed with the results obtained from the 3D model calculations.

The filters were designed with the Filter Design & Analysis Tools (fdatool) included in the Signal Processing Toolbox in MATLAB R2009b, and according to the data in the table below.

	3D Models	2D Model
Sampling frequency (kHz)	7.1	8.6
Passband frequency (Hz)	950	1800
Stopband frequency (kHz)	3.5	4
Passband ripple (dB)	3	3
Stopband attenuation (dB)	40	40

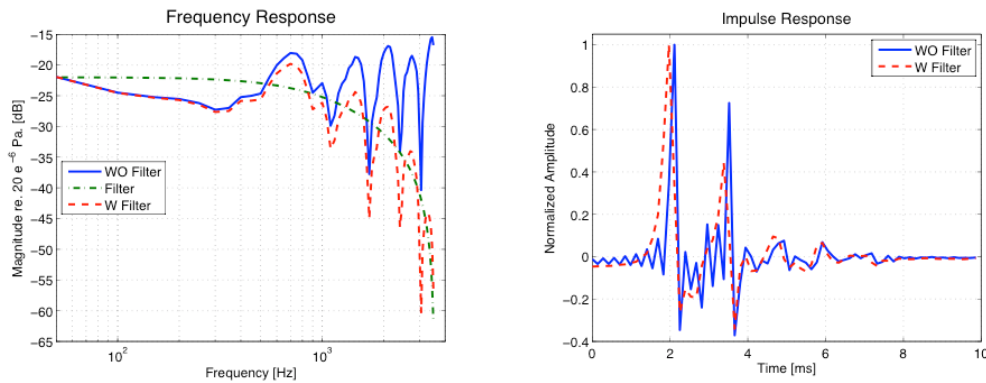


**Figure 8: Filter effects on the Frequency Response (left) and on the Impulse Response (right). “WO Filter” (continuous line) stands for without filter and “W Filter” (dashed line) stands for with filter. “Filter” (dotted-dashed line) is the low-pass Butterworth filter response.**

Figure 8 illustrates the filter effects on the frequency (left side) and impulse responses (right side). The frequency response, left side, shows how the response, continuous line, is attenuated by the filter response, dotted-dashed line, the dashed line is the response with the filter and the dot-dashed line is the filter response.

3D Butterworth Low-pass filter is a first order, and was designed according to the next data:

- Sampling frequency: 7.1 kHz
- Passband frequency: 950 Hz
- Stopband frequency: 3.5 kHz
- Passband ripple (dB): 3 dB
- Stopband attenuation (dB): 40 dB
- 

2D Butterworth Low-pass filter is of second order, and was designed with the next parameters:

- Sampling frequency: 8.6 kHz
- Passband frequency: 1.8 kHz
- Stopband frequency: 4 kHz
- Passband ripple (dB): 3 dB
- Stopband attenuation (dB): 40 dB

The frequency responses of these filters are shown in Figure 9.

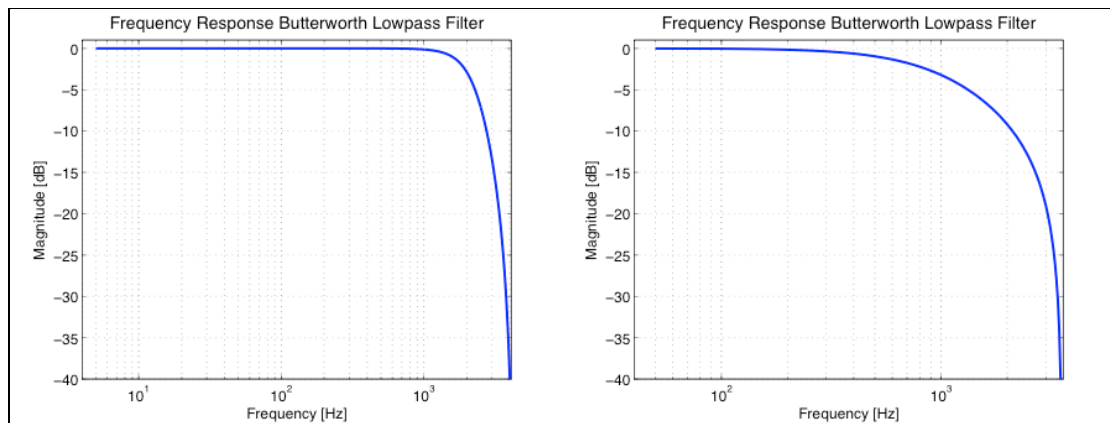


*Figure 9: Butterworth low-pass filter. Left - 2D Model. Right - 3D Model.*

## 4. Results

In this chapter the general findings are presented. The first section shows the results of the 2D model. In the second section the results of the 3D model are provided.

The FEM results will be the IR when in most of the cases the results are the FRF and/or the eigenfrequencies and the eigenmodes.

### Enclosed Air Space 2D Model

Figure 7 depicts the findings of the 2D model.

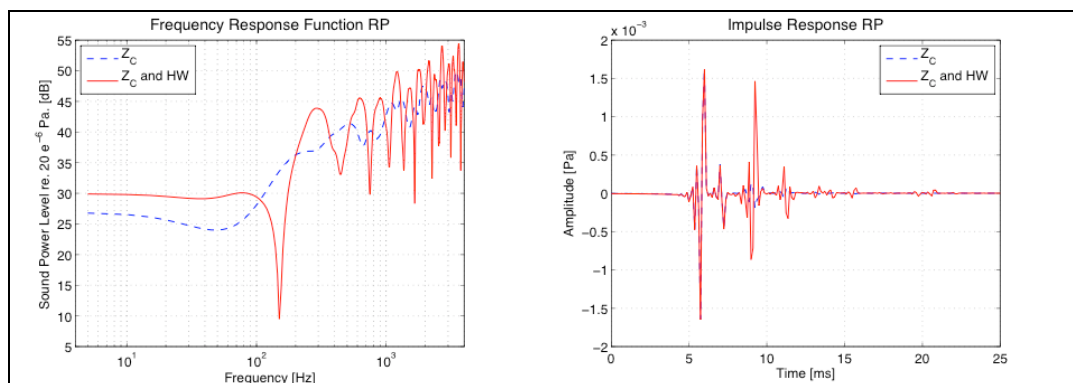


**Figure 10: 2D model simulation results at receiver position. Left - Frequency Response Function. Right - Impulse Response Function**

# Passenger Car Compartment 3D Models

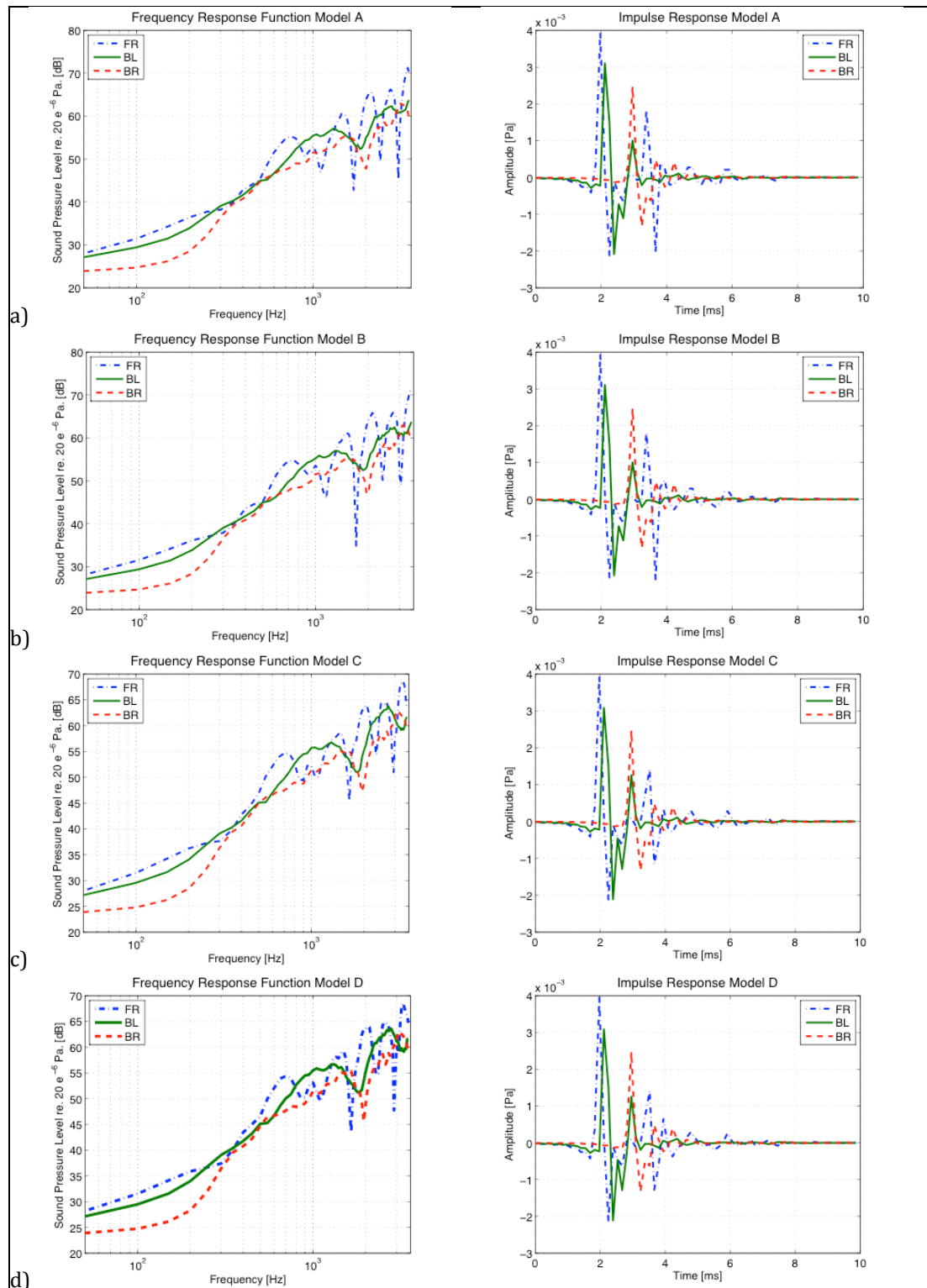


Figure 11: 3D simulation results at receiver positions. Left - Frequency Response Function. Right - Impulse Response Function. a) Model A. b) Model B. c) Model C. d) Model D.

## 5. Discussion

Figure 9 to 10 show the FRF and IRF at each receiver position. The results correspond to the sound waves reflected by the side windows and the windshield. It is easy to see the differences produced by the changes in the windshield and side windows geometries.

In the FRF plots the dips at certain frequencies become more prominent as the receiver position changes, suggesting a strong dependency of the sound field on the direct wave path. The differences in sound pressure level increase as the frequency increases, insinuating, as expected, that the geometry changes has a strong influence at higher frequencies.

For the front right position models A and B have the same trend, whereas models C and D behave the same, allowing to think that the side windows geometry has a strong influence on the sound field.

For the back left position it is complicated to indicate which surface affects more the sound field. It seems that at this position the sound field is affected more by the direct path than by changes in geometry.

For the back right position the tendency is mixed. At certain frequencies Models B and D look similar, at others models A and C. All seems to be a combination and the geometry shapes affect the sound field in a combined way.

In the IR it is possible to identify the reflections arriving at every receiver position.

For the front right position the first impulse is dominated by the geometries of the side windows. For the subsequent reflections it is a little bit complicated to identify where the reflection is coming from.

For the back left and back right positions the side windows affect the sound field more than the windshield geometry.

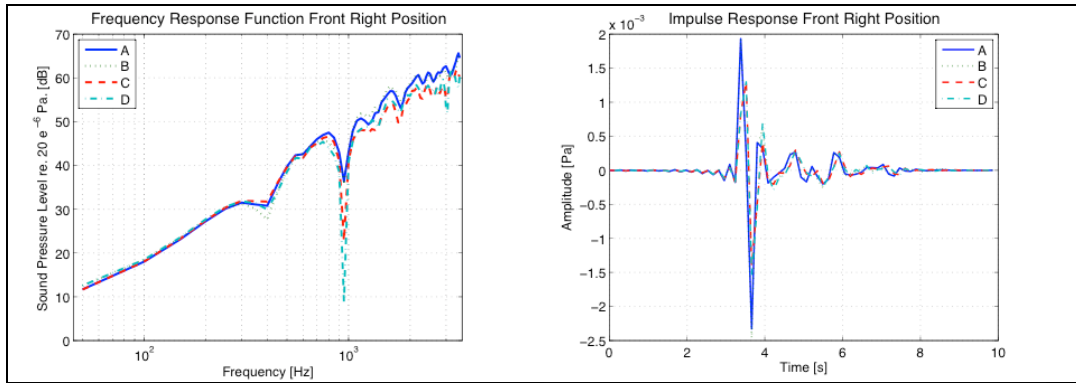


**Figure 12: 3D model results at the Front Right Position. Left - Frequency Response Function. Right - Impulse Response Function**

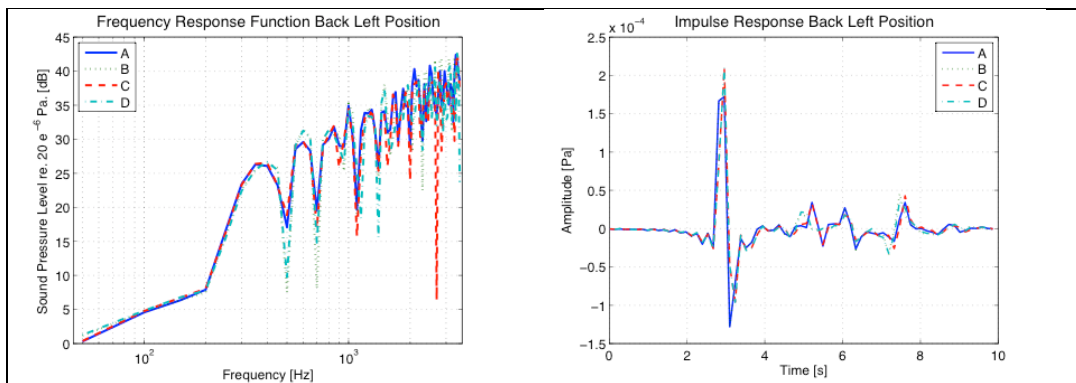


**Figure 13: 3D model results at the Back Left Position. Left - Frequency Response Function. Right - Impulse Response Function**

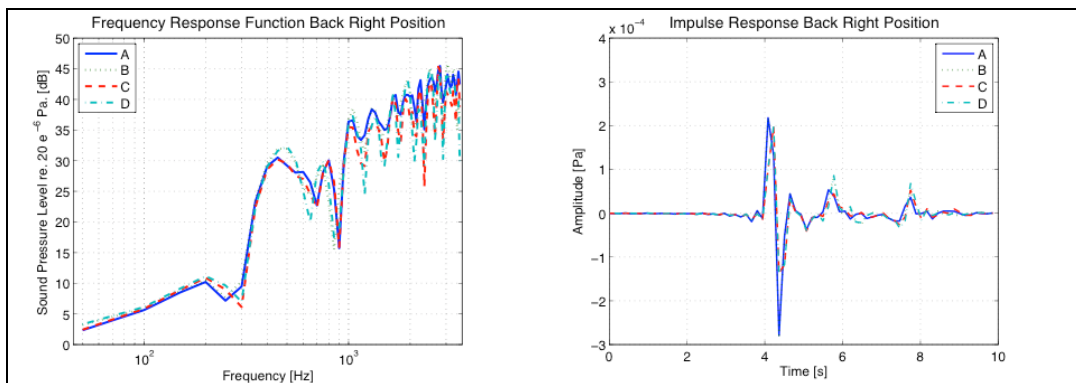


**Figure 14: 3D model results at the Back Right Position. Left - Frequency Response Function. Right - Impulse Response Function**

## 6. Conclusions

The four models in this work were based on the 9-3 Saab passenger compartment. To obtain the reflected waves coming from the side windows and the windshield a set of different boundary conditions was used. The FEM calculated transfer functions coupled with the Butterworth low pass filter characteristic windowing enabled the calculation of causal physically relevant impulse responses. This would not have been possible using ray tracing or image source modelling.

## 7. Future Work

Since the present project was done using simplified passenger compartment models under quite basic assumptions there are many opportunities for future work as:

- a. Validate the simulation results by comparison to measurement results. It was not possible to validate the simulation results with actual measurements of passenger compartments because the results obtained from the simulations correspond to very simplified models. Therefore the measurements must be performed in an anechoic chamber using three sound hard surfaces that would represent the windshield and front side windows.
- b. Replace the single receiver points by an array of points. With this change it would be possible to identify and have more information about the surfaces that are reflecting sound.
- c. Increase the upper frequency limit in the simulations. It has been shown that the low-pass filter helps to get rid of non-causality effects in the impulse responses, but at the same time it reduces the amount of information provided by the frequencies above the passband frequency. Hence having a higher upper frequency limit would grant enough data even if a filter were applied.
- d. Include in the models absorption coefficients or flow resistivity values of the different surfaces in order to simulate an environment much more alike to the one present inside a real passenger compartment.
- e. Replace the point source by a source with a directivity pattern similar to human voice by including a “real” head geometry in the FEM model.

## 8. Bibliography

- [1] A. Craggs. "The Use of Simple Three-Dimensional Acoustic Finite Elements for Determining the Natural Modes and Frequencies of Complex Shaped Enclosures." *Journal of Sound and Vibration* 23, no. 3 (1972): 331-339.
- [2] A. Muğan, G. M. Hulbert. "Nonreflecting Boundary Conditions in Acoustics for Finite Element Methods Based Upon Off-surface Boundary Integral Equations." *Computer Methods in Applied Mechanics and Engineering* 188 (2000): 289-306.
- [3] A. Pietrzyk, M. Kleiner. "The Application of the Finite Element Method to the Prediction of Sound Fields of Small Rooms at Low Frequencies." *Presented at the 102nd Convention*. Munich, Germany: AES, 1997. 4423.
- [4] B. van Genechten, B. Pluymers, D. Vandepitte and W. Desmet. "A Hybrid Wave Based - Modally Reduced Finite Element Method for the Efficient Analysis of Low and Mid Frequency Car Cavity Acoustics." *SAE International Journal of Passenger Cars - Mechanical Systems* 2, no. 1 (October 2009): 1494-1504.
- [5] B. van Hal, W. Desmet, D. Vandepitte, P. Sas. "Hybrid Finite Element - Wave Based Method for Acoustic Problems." *Computer Assisted Mechanics and Engineering Sciences* 10, no. 4 (2003): 479-494.
- [6] D. J. Nefske, J. A. Wolf, L. J. Howell. "Structural-Acoustic Finite Element Analysis of the Automobile Passenger Compartment: A Review of Current Practice." *Journal of Sound and Vibration* 80, no. 2 (1982): 247-266.
- [7] D. J. Nefske, S. H. Sung, A. E. Duncan. "Application of Finite Element Methods to Vehicle Interior Acoustic Design." *SAE Document Number 840743*, April 1984: 197-205.
- [8] E. Granier, M. Kleiner, B.-I. Dalenbäck and P. Svensson. "Experimental Auralization of Car Audio Installations." *Journal of the Audio Engineering Society* 44, no. 10 (October 1996): 835-849.
- [9] F. Ihlenburg. "The Medium-Frequency Range in Computational Acoustics: Practical and Numerical Aspects." *Journal of Computational Acoustics* 11, no. 2 (2003): 175-193.

- [10] G. C. Everstine. "Finite Element Formulations of Structural Acoustic Problems." *Computers and Structures* 65, no. 3 (November 1997): 307-321.
- [11] G.M.L. Gladwell. "A Finite Element Method for Acoustics." *5th International Congress on Acoustics* (September 1965): L33.
- [12] J. B. Keller, D. Givoli. "Exact Non-reflecting Boundary Conditions." *Journal of Computational Physics* 82 (1989): 172-192.
- [13] J. Biermann, O. von Estoff, S. Petersen, C. Wenterodt. "Higher Order Finite and Infinite Elements for the Solution of Helmholtz Problems." *Computer Methods in Applied Mechanics and Engineering* 198 (2009): 1171-1188.
- [14] J. Mørkholt, J. Hald, P. Hardy, D. Trentin, M. Bach-Andersen and G. Keith. "Measurements of Absorption Coefficient, Surface Admittance, Radiated Intensity and Absorbed Intensity on the Panels of a Vehicle Cabin using a Dual Layer Array with Integrated Position Measurement." *SAE International Journal of Passenger Cars - Mechanical Systems* 2, no. 1 (October 2009): 1449-1457.
- [15] K. H. Huebner, D. L. Dewhurst, D. E. Smith, T. G. Byron. *The Finite Element Method for Engineers*. 4th Edition. New York: Wiley, 2001.
- [16] L. L. Thompson. "A Review of Finite-Element Methods for Time-Harmonic Acoustics." *Journal of the Acoustical Society of America* 119, no. 3 (March 2006): 1315-1330.
- [17] M. A. Jamnia, C. Rajakumar. "An Acoustic Design Optimization Technique for Automobile Audio Systems." *SAE Transactions* 98, no. 6 (1989): 229-239.
- [18] M. Petyt, J. Lea and G.H. Koopmann. "A Finite Element Method for Determining the Acoustic Modes of Irregular Shaped Cavities." *Journal of Sound and Vibration* 45, no. 4 (1976): 495-502.
- [19] O. C. Zienkiewicz. "Achievements and Some Unsolved Problems of the Finite Element Method." *International Journal for Numerical Methods in Engineering* 49 (2000): 9-28.
- [20] O. C. Zienkiewicz. *The Finite Element Method in Engineering Science*. London: Mc-Graw Hill, 1971.

- [21] O. C. Zienkiewicz, R. L. Taylor and P. Nithiarasu. *The Finite Element Method – Volume 1: Basic formulation and linear problems*. Oxford; New York: Elsevier/ Butterworth-Heinemann, 2005.
- [22] O. Cessenat, B. Després. "Using Plane Waves as Base Functions for Solving Time Harmonic Equations with the Ultra Weak Variational Formulation." *Journal of Computational Acoustics* 11, no. 2 (2003): 227-238.
- [23] P. L. Arlett, A. K. Bahrani, and O. C. Zienkiewicz. "Application of Finite Elements to the Solution of Helmholtz's Equation." *Proc. IEEE* 15, no. 12 (1968): 1762-1766.
- [24] P. M. Gauzellino, F. I. Zyserman, J. E. Santos. "Nonconforming Finite Element Methods for the Three-Dimensional Helmholtz Equation: Iterative Domain Decomposition or Global Solution?" *Journal of Computational Acoustics* 17, no. 2 (2009): 159-173.
- [25] P. M. Morse, K. U. Ingard. *Theoretical Acoustics*. New York: McGraw-Hill, 1968.
- [26] Q. Di, M. Zhang, M. Wang. "Time-Domain Finite-Element Wave Form Inversion of Acoustic Wave Equation." *Journal of Computational Acoustics* 12, no. 3 (2004): 387-396.
- [27] R. H. Bolt, H. Feshbach and A. M. Clogston. "Perturbation of Sound Waves in Irregular Rooms." *Journal of the Acoustic Society of America* 13 (1942): 65-73
- [28] S. Choi and H Tachibana. "Estimation of Impulse Response in a Sound Field by the Finite Element Method." *13th International Congress on Acoustics* 2 (1989): 129-132.
- [29] S. H. Sung. "Automotive Applications of Three-Dimensional Acoustic Finite Elements." *SAE Document Number 810397*, February 1981: 1-12.
- [30] S. Marburg. "Six Boundary Elements per Wavelength: Is That Enough?" *Journal of Computer Acoustics* 10, no. 1 (2002): 25-51.
- [31] T. J. Cox and P. D'Antonio. *Acoustic Absorbers and Diffusers. Theory, design and application*. New York: Spon Press, 2004.

- [32] T. L. Richards, S. K. Jha. "A simplified Finite Element Method for Studying Acoustic Characteristics Inside a Car Cavity." *Journal of Sound and Vibration* 63, no. 1 (1979): 61-72.
- [33] T. Shuku and K. Ishihara. "The Analysis of the Acoustic Field in Irregularly Shaped Rooms by the Finite Element Method." *Journal of Sound and Vibration* 29, no. 1 (1973): 67-76.
- [34] W. Bangerth, R. Rannacher. "Adaptive Finite Element Techniques for the Acoustic Wave Equation." *Journal of Computational Acoustics* 9, no. 2 (2001): 575-591.
- [35] "Acoustics Module User's Guide." COMSOL Multiphysics, November 2008.
- [36] "COMSOL Multiphysics User's Guide." COMSOL Multiphysics, November 2008.

# Appendix A

## Car Compartment Geometries

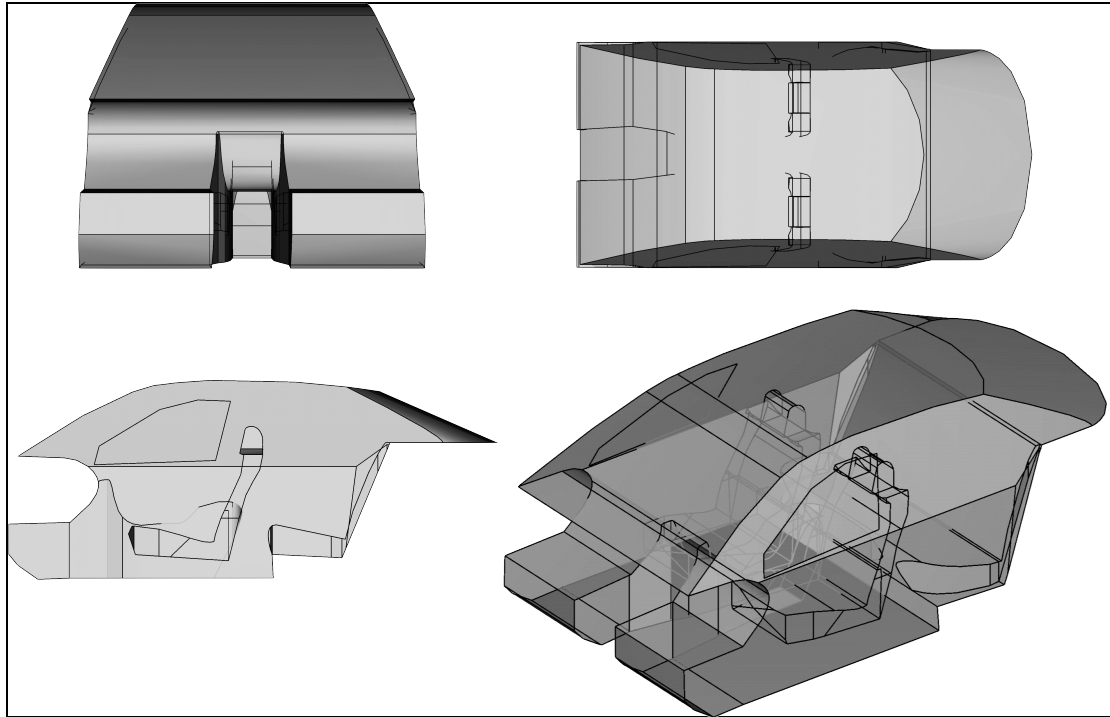


*Figure A1: Model A*

Figure 15 Model D with two head and torso simulators

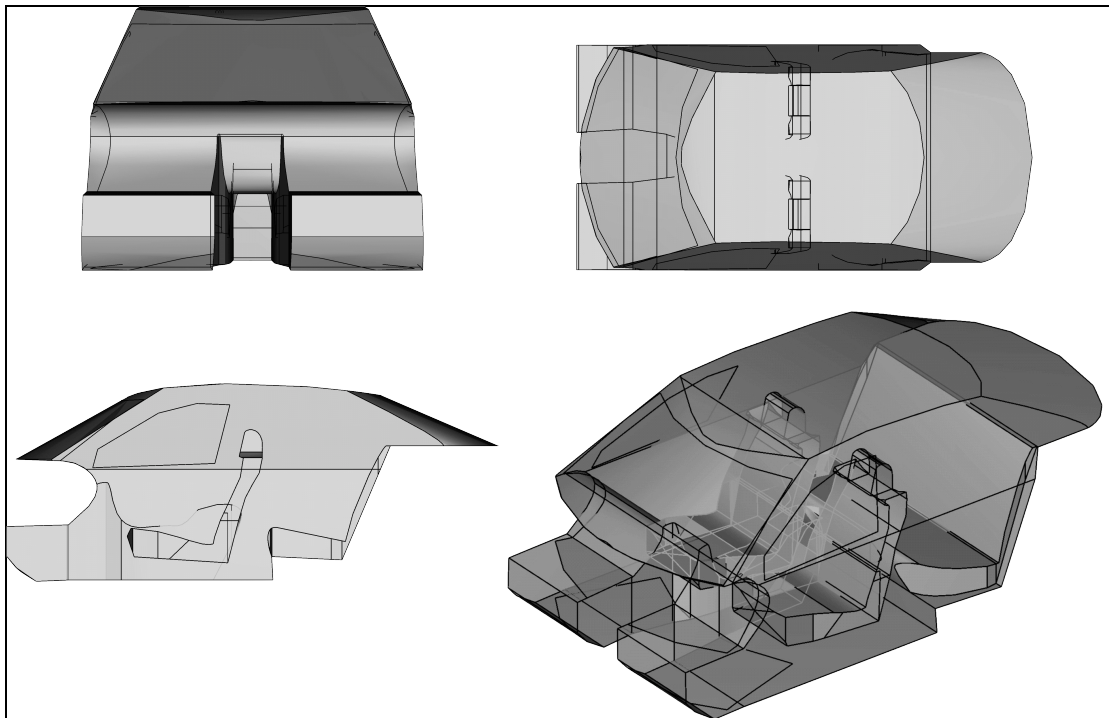
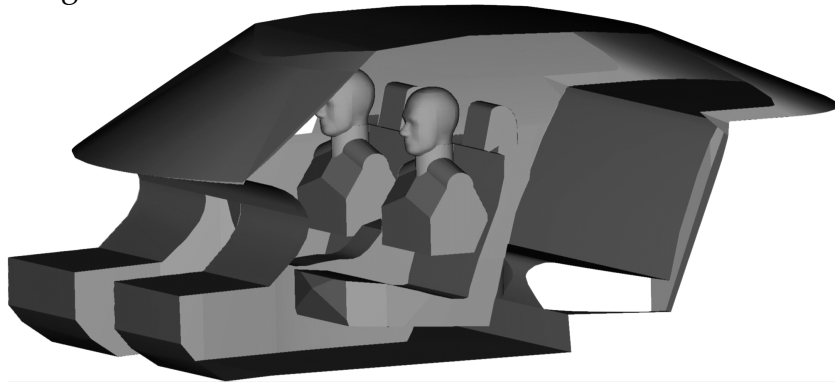
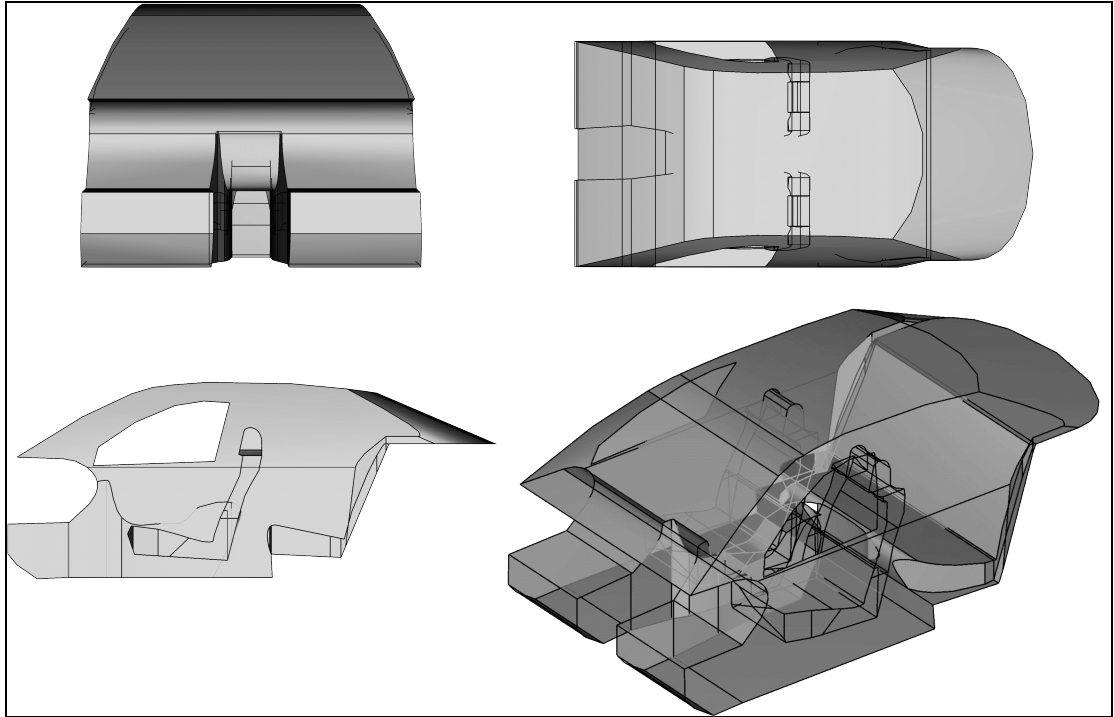
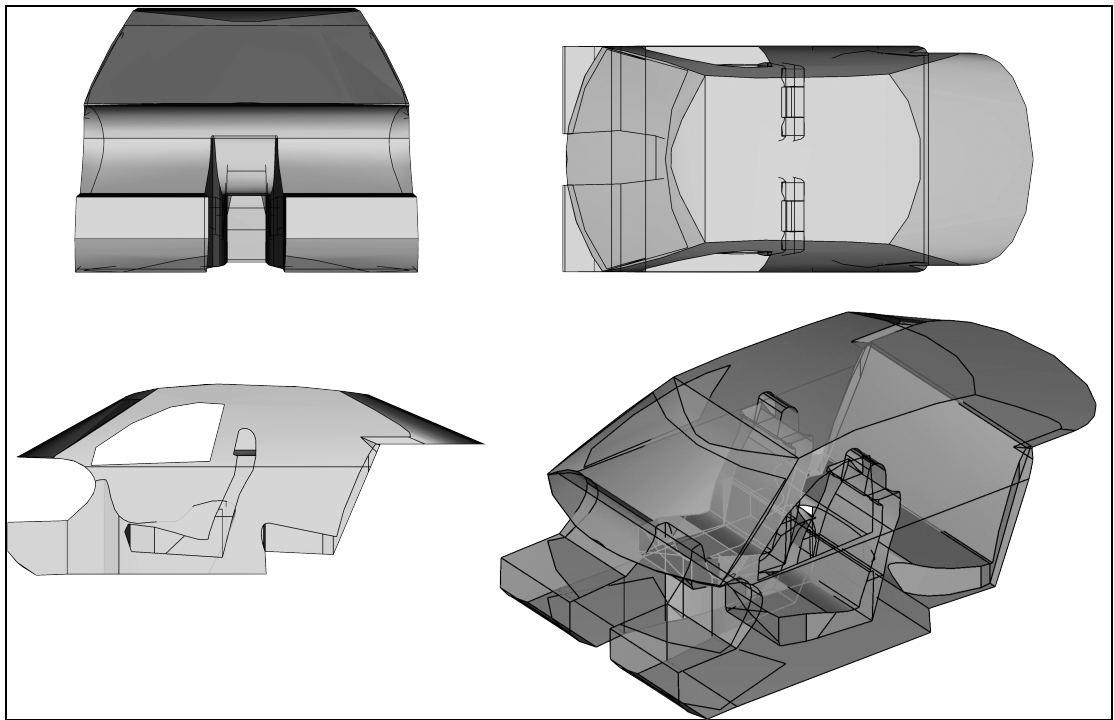


Figure A2: Model B



*Figure A3: Model C*



*Figure A4: Model D*